Journal of Earth Sciences and Geotechnical Engineering, vol. 3, no. 2, 2013, 1-19
ISSN: 1792-9040 (print), 1792-9660 (online)
Scienpress Ltd, 2013

General Approaches of Solving Seismic Source Dynamic Parameters and Q Value of the Medium

Wenlong Liu[1] and Yucheng Liu[2]

Abstract

This paper presents general approaches and numerical models of solving seismic dynamic parameters and determining medium's quality factor. The methods presented here can be extensively applied to investigate characteristics of existing seismic waves so as to obtain correct prediction of forthcoming earthquakes and judgment of seismic tendency in certain regions. Errors in estimating different seismic parameters are also discussed, which may be caused by different reasons.

Keywords: Hypocentral radius, stress drop, ambient shear stress, rupture characteristics, Q value

1 Introduction

Seismic source dynamic parameters carried by seismic waves have received growing research interests because the variation of those parametric values not only reflect the characteristics of current seismicity but also reveal the future seismic tendency in certain regions. Therefore, those parameters have wide applicability in earthquake prediction. In order to correctly estimate those seismic source parametric values, different physical models and approaches have been developed. This paper reviews approaches and models that are commonly used for calculating seismic parametric values such as hypocentral radius, stress drop, ambient shear stress, medium's Q value, and rupture characteristics. General physical models and approaches discussed in this paper include circular dislocation model, Brune model, explosive source model, uni- and bilateral finite moving source model, instrumental and medium calibration, and directional function. Methods for earthquake selection, sampling and Fourier analysis are also introduced in this paper. In addition, error analysis is performed to discuss the errors that are generated in estimating those parameters. It is accepted that error estimation must be provided along with the earthquake prediction in order to make the predictions more reliable and convincing.

[1]Shanghai Earthquake Administration.
[2]University of Louisiana at Lafayette.

2 Solve Hypocentral Radius, Stress Drop, and Ambient Shear Stress

2.1 Using Circular Dislocation Model

There two equivalent approaches to regress the hypocenter from seismic record using earthquake source model. Here we use P wave for an example. One way is to compose the seismogram based on parameters of the given hypocentral and medium models, which is performed within time domain (Eqn. (1)).

$$R_\alpha(t) = I(t) * B(t) * u_\alpha(t) \tag{1}$$

where "*" represents convolution; $R_\alpha(t)$ is theoretical displacement diagram of seismic body waves; I(t) and B(t) are instrumental and medium impulse response functions, respectively; $u_\alpha(t)$ is displacement of seismic body waves of hypocentral radiation. The parameters of hypocentral and medium models can be adjusted so that the theoretical seismogram will be consistent with the recorded seismogram and the hypocentral parameters then can be estimated. In doing this, several masks is first made for the used instrumental parameters and then the quality factor of medium Q can be solved from the masks according to the minimum half period of P waves of a large amount of local small earthquakes. Hypocentral radius a can be found from the masks based on the half period of initial motion of the studied earthquake, $t_{2\alpha}$. From a and the amplitude of initial motion of the earthquake $u_{\alpha m}$, the seismic moment m_0 will eventually be found. For more details about this method, please refer to [1].

The other method is performed within frequency domain, which is to first find Fourier transformation of the recorded seismogram and to obtain the displacement spectrum of earthquake source radiation (Eqn. (2) and Figure 1) after removing the influences of medium and instrument.

$$\hat{u}_\alpha(\omega) = \frac{\hat{R}_\alpha(\omega)}{\hat{I}(\omega) \cdot \hat{B}(\omega)} \tag{2}$$

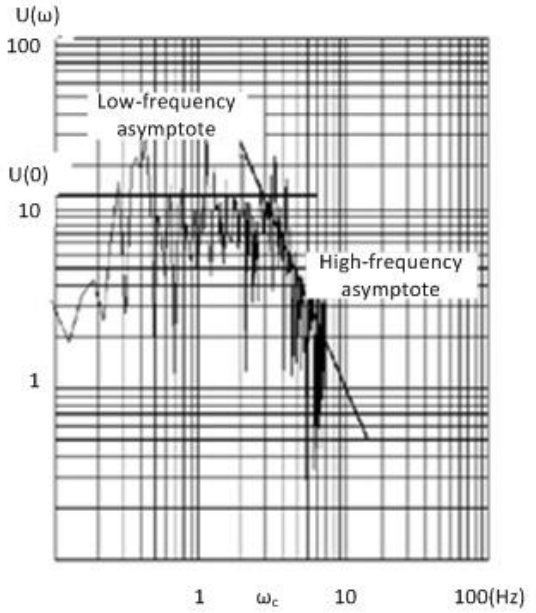

Figure 1: Spectrum of earthquake source

Based on the two eigenvalues of the spectral curve, intersection between the low-frequency asymptote and the vertical axis $\hat{u}_\alpha(0)$, and the corner frequency $f_{c\alpha}$, the seismic moment m_0 and hypenctral radius a can be determined as:

$$\begin{cases} a = \dfrac{1.45\alpha}{2\pi f_{c\alpha}} \\ m_0 = \dfrac{4\pi\rho\alpha^3 r|\hat{u}_\alpha(0)|}{\Re_\alpha} \end{cases} \tag{3}$$

where $\Re_\alpha$ uses the mean value on the focal sphere (at 45º), $(4/15)^{1/2}$. For an S wave, that mean value $\Re_\beta$ is $(2/15)^{1/2}$.

Finally, stress drop, average dislocation and maximum dislocation can be determined based on m_0 and a as:

$$\begin{cases} \Delta\bar{u} = \dfrac{m_0}{\mu \cdot A} \\ \Delta\sigma = \eta \dfrac{\mu \cdot \Delta u_m}{a} = \eta' \dfrac{\mu \cdot \Delta u}{a} \end{cases} \tag{4}$$

where A is the area of dislocation surface, η and η' take different values with respect to different dislocation surface.

For example, if we use Keilis-Borok mode for circular shear dislocation model, then we have:

$$\begin{cases} \Delta\sigma = \dfrac{7m_0}{16a^3} \\ \Delta\bar{u} = \dfrac{16\Delta\sigma \cdot a}{7\pi\mu} \\ \Delta u_m = \dfrac{3\Delta\bar{u}}{2} \end{cases} \tag{5}$$

Based on classic theory of fracture mechanics we can have:

$$\begin{cases} m_o = \dfrac{(1-\nu)\pi\tau_0^2(2a)^3}{3(2-\nu)\tau_y} \\ M_s = 2\lg(2a) + \dfrac{1}{1.5}\left[\dfrac{\lg 4(1-\nu)\tau_0^2\eta}{3(2-\nu)\mu} - 11.8\right] \\ \dfrac{\Delta\bar{u}}{2a} = \dfrac{4(1-\nu)\tau_0^2}{3(2-\nu)\pi\mu\tau_y} \end{cases} \tag{6}$$

From above equations the ambient shear stress τ_0 can be solved.

2.2 Instrumental and Medium Calibration

Instrumental calibration

$\hat{I}(\omega)$ in Eqn. (2) is frequency characteristic of the instruments. For an analog seismograph, its frequency characteristic equals the product of the frequency characteristics of seismometer pier $\hat{I}_1(\omega)$, amplifier $\hat{I}_2(\omega)$, and pen point $\hat{I}_3(\omega)$

$$\hat{I}(\omega) = \hat{I}_1(\omega) \cdot \hat{I}_2(\omega) \cdot \hat{I}_3(\omega) = W(\omega) \cdot e^{-i\Phi(\omega)} \tag{7}$$

where W(ω) is amplitude-frequency characteristic, ϕ(ω) is phase-frequency characteristic. SK seismograph and VGK seismograph had been the two primary seismometers used in China until last 70's. In 1970's, large-scale local seismic networks were established in China and short-period seismographs such as model 64, 65, 63A, 67 (linear amplifier) and micro seismographs such as DD-1 and DK-1 seismographs were successively used since then. Since end of the 20th century and beginning of the 21st century, digitized seismographs have emerged and gradually replaced the traditional analog seismographs, and most seismic data were recorded by model 64(65) and DD-1(DK-1) seismographs. This section provides fundamental parameters for those instruments.

(1) Horizontal SK seismograph: period of pendulum T_1 = 12.0 sec, its damping ratio D_1 = 0.45, period of amperemeter T_2 = 11.1 sec, its damping ratio D_2 = 5.5, coupling coefficient σ^2 = 0.079, and the impulse response is:

$$I(t) = \frac{\bar{k}}{l_0}\left\{1.015e^{-61.78t} - 0.0065e^{-0.487t} + 2e^{-0.224t}\left[-0.00435\cos(0.486t) - 0.00121\sin(0.486t)\right]\right\} \tag{8}$$

where $\frac{\bar{k}}{l_0}$ = 1 for calculation.

(2) VGK seismograph: T_1 = 1.0 sec, D_1 = 0. 5, T_2 = 0.1 sec, D_2 = 8.0, σ^2 = 0.4, and the impulse response is

$$I(t) = \frac{\bar{k}}{l_0}\left\{1.00076e^{-10039t} - 0.00065e^{-3.11t} + 2e^{-2.28t}\left[-0.00349\cos(6.68t) - 0.00175\sin(6.68t)\right]\right\} \tag{9}$$

(3) DD-1 and DK-1 seismograph: amplitude-frequency characteristic is:

$$W(\omega) = \frac{\omega_\tau^3 \tau_1 \tau_2}{\sqrt{\left(1+\tau_1^2\omega^2\right)\left(1+\tau_2^2\omega^2\right)\left(1+\tau^2\omega^2\right)\left\{\left[1-\left(\frac{\omega_s}{\omega}\right)^2\right]^2 + 4D_s^2\left(\frac{\omega_s}{\omega}\right)^2\right\}\left\{\left[1-\left(\frac{\omega}{\omega_B}\right)^2\right]^2 + 4D_B^2\left(\frac{\omega}{\omega_B}\right)^2\right\}}} \tag{10}$$

Phase-frequency characteristic is:

$$\Phi(\omega) = arctg\frac{2D_s\frac{\omega_s}{\omega}}{1-\left(\frac{\omega_s}{\omega}\right)^2} + \frac{\pi}{2} - arctg\frac{2D_B\frac{\omega}{\omega_B}}{1-\left(\frac{\omega}{\omega_B}\right)^2} - arctg\tau\omega + arctg\frac{1}{\tau_1\omega} + arctg\frac{1}{\tau_2\omega} \tag{11}$$

For more parameters about DD-1 and DK-1, please see Table 1, where $\omega_{s,B} = 2\pi f_{s,B}$

Table 1: Instrumental parameters of DD-1 and DK-1 seismograph

Model type	τ	τ_1	τ_2	F_s	D_s	f_B	D_B
DD-1	0.22	0.84	0.80	1	0.45	20	0.707
DK-1	5.0	16.0	8.0	0.067	0.45	20	0.707

(4) Short-period seismograph: amplitude-frequency characteristic is:

$$W(f) = K \cdot f \cdot Q_s(f) \cdot Q_{BG}(f) \cdot S_B(f_B) \tag{12}$$

where

$$\begin{cases} Q_s(\omega) = 1/\sqrt{\left[1-\left(\dfrac{\omega_s}{\omega}\right)^2\right]^2 + 4D_s^2\left(\dfrac{\omega_s}{\omega}\right)^2} \\ Q_{BG}(f) = 1/\sqrt{1+\dfrac{\left[(f/f_B)^2-1\right]^2}{4D_B^2(f/f_B)^2}} \\ S_B(f_B) = \dfrac{G_B}{8\pi^2 D_B \cdot J_B \cdot R_B \cdot f_B^2} \end{cases} \tag{13}$$

and

$$Q_{BG}(f) = 1/\sqrt{4D_B^2(f/f_B)^2 + \left[1-(f/f_B)^2\right]^2} \tag{14}$$

Phase-frequency characteristic is:

$$\Phi(f) = \Phi_s(f) + \frac{\pi}{2} + \Phi_f(f) + \Phi_B(f) \tag{15}$$

where

$$\begin{cases} \Phi_s(\omega) = arctg\, 2D_s\left(\dfrac{\omega_s}{\omega}\right) \Big/ \left[1-\left(\dfrac{\omega_s}{\omega}\right)^2\right]^2 \\ \Phi_f = \begin{cases} \pi \\ 0 \end{cases} \\ \Phi_B(f) = arctg\left(2D_B\dfrac{\omega}{\omega_B}\right) \Big/ \left[1-\left(\dfrac{\omega}{\omega_B}\right)^2\right]^2 \end{cases} \tag{16}$$

In above equations, G_B is electric constant and J_B is moment of inertia. Other parameters are listed in following table.

Table 2: Instrumental parameters for short-period seismographs

Model type	f_s	D_s	f_B	D_B
Model 64	1/(1.0 ~ 1.5)	0.5	5 ~ 7 Hz	JFB-2
Model 65	1	0.5	1/0.14	1.5 ~ 3

Medium calibration

Medium has influences on three facets: absorption, frequency dispersion, and free surface. Assuming the reflected wave of a free surface equals to its incident wave, the medium influence can be represented as the source displacement spectrum being multiplied by a scale factor 2. The influence on absorption can be expressed as the source displacement

spectrum being multiplied by a factor $e^{-\frac{\omega r}{2cQ}}$, where c is the velocity of body wave. The influence on frequency dispersion is similar to that on absorption except that the velocity c is replaced by the phase velocity c_P, which is:

$$c_P = c \Big/ \left(1 - \frac{1}{2\pi Q} \ln \left| \left(\frac{\omega}{\omega_0}\right)^2 - 1 \right| \right) \tag{17}$$

where ω_0 is the low cutoff frequency. Thus, the overall medium influence on absorption, dispersion and free surface should be:

$$\hat{B}(\omega) = 2e^{-\frac{\omega r}{2cQ} + i\frac{\omega r}{2\pi cQ} \ln \left| \left(\frac{\omega}{\omega_0}\right)^2 - 1 \right|} \tag{18}$$

2.3 Earthquake Selection, Sampling and Fourier Analysis

In preparing analog seismograph, appropriate seismic data is required. The selected earthquake samples can neither be too big nor too small. If an earthquake is too big, its record may exceed space of seismograph. On the contrary, small earthquakes will lead to high error and may be seriously influenced by instruments and medium. Meanwhile, epicentral distance of the selected earthquakes cannot be too short; otherwise the recorded seismic waveforms will be too close to be discretized. In addition, usable seismograph has to be clear, no breakage, and a wave band has to be recorded in a single line. Because of those constraints, only less than half of the analog seismic records can be used for spectral analysis while digital seismic records do not have such problems.

There are two important sampling parameters: step size Δt and window length T. Nyquist frequency is dependent on the step size as $f_{n/2} = 1/(2\Delta t)$. If seismic data has frequency components higher than the Nyquist frequency, those frequency components cannot be detected. Even worse, the existence of the high frequency components will cause remarkable error, called as high frequency aliasing. Therefore, in selecting Δt, we need to make sure that $f_{n/2}$ is higher than the highest frequency component f_{max} of the seismic data. Meanwhile, in order to correctly identify high frequency progressiveness, f_{max} should be evidently higher than the corner frequency f_c.

Fundamental frequency of spectrum can be determined as $f_{min} = 1/T$, where $T = N\Delta t$ is the window length and N is total number of sampling points. Spectral analysis is then performed on seismic data F(t) during the time period T, which is:

$$f(t) = F(t)W(t) \tag{19}$$

$$W(t) = \begin{cases} 1 \ldots\ldots -T/2 \le t \le t/2 \\ 0 \ldots\ldots t < -T/2, t > T/2 \end{cases} \tag{20}$$

W(t) is the time window, which is also called rectangular window in here (Fig. 2). Fourier spectrum of f(t) is the convolution of the Fourier spectra of F(t) and W(t).

$$\begin{cases} \hat{f}(\omega) = \hat{F}(\omega) * \hat{W}(\omega) \\ \hat{W}(\omega) = 2\sin T/\omega T \end{cases} \tag{21}$$

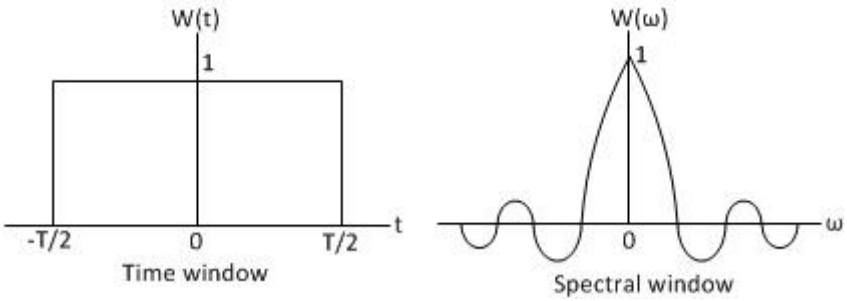

Figure 2: Rectangular window and its spectral window

In Figure 2, the peak width in the middle of the spectral window is called bandwidth and the small undulations on both sides are called sideband. From Eqn. (21) it is known that the smaller the bandwidth and sideband are, the more accurate spectrum will be solved. Therefore, the rectangular window is not an ideal window for Fourier analysis because of its comparatively large sideband. In practice, the two most frequently-used windows in Fourier analysis are Hanning window (Eqn. (22)) and Hamming window (Eqn. (23)).

$$\begin{cases} W(t) = \begin{cases} \dfrac{1}{2T}\cdot\left(1+\cos \pi t/T\right),...0 \le t \le T \\ 0,.....t > T \end{cases} \\ \hat{W}(\omega) = \dfrac{\sin \omega T}{\omega T} + \dfrac{1}{2}\left[\dfrac{\sin(\omega T+\pi)}{\omega T+\pi} + \dfrac{\sin(\omega T-\pi)}{\omega T-\pi}\right] \end{cases} \tag{22}$$

$$\begin{cases} W(t) = \begin{cases} \dfrac{1}{T}\cdot\left(0.54+0.46\cos \pi t/T\right),.....0 \le t \le T \\ 0,.....t > T \end{cases} \\ \hat{W}(\omega) = 1.08\dfrac{\sin \omega T}{\omega T} + 0.46\left[\dfrac{\sin(\omega T+\pi)}{\omega T+\pi} + \dfrac{\sin(\omega T-\pi)}{\omega T-\pi}\right] \end{cases} \tag{23}$$

From above equations it can be found that in order to reduce the bandwidth, a large window length T should be used. Based on our experience, it is agreed that an ideal T should be as 8 to 10 times as reciprocal of the corner frequency f_c without mixing with other waves ($T \approx 8\text{-}10(1/f_c)$).

Sampling can be performed on a stereocomparator but it will be much easier to use a scanner for sampling with the help of the seismogram digitization and database management system (SDDMS) [2]. Generally the basic axis of sampling does not overlap with the baseline of the recording chart, so the inclining and zero-frequency components have to be firstly removed after digitalization. Also, since the recorded data are arcs, the large amplitude radians have to be modified. In order to do that, large amplitudes between t_1 and t_2 are measured every equal amplitude-space, then interpolation are performed among these measurements and t_1 and t_2 to obtain an unequal time-space sampling. Next, connecting those samples through lines and redo an equal time-space sampling. (These steps are not needed if using digital record.) Afterwards, fast Fourier transformation (FFT) is performed using Hanning window to obtain all samples and the total number of the samples must be two of integral power (2^n). Finally, the seismic spectrum radiated from the hypocenter can be acquired after instrumental and media calibration.

2.4 Solve for Hypocentral Radius and Stress Drop

2.4.1 Brune model

Based on the recorded displacement response spectrum of S-wave and eliminating the influences of instruments and medium, the S-wave spectrum at hypocenter can be obtained as:

$$\hat{u}_\beta(r,\omega)=\frac{\hat{R}_\beta(\omega)}{\hat{I}(\omega)\cdot\hat{B}(\omega)}=\Re_\beta\cdot\frac{a}{r}\cdot\frac{\Delta\sigma\cdot\beta}{\mu}\cdot\frac{1}{\omega^2+\omega_c^2} \tag{24}$$

From the low-frequency level of the S-wave spectrum, m_0 can be determined as

$$m_0=4\pi\rho\beta^3 r\cdot\left|\hat{u}_\beta(0)\right|/\Re_\beta \tag{25}$$

where $\Re_\beta$ choose the average value on the focal spherical surface (at 45º), $(2/5)^{1/2}$. The radius of rupture plane a can be calculated from the corner circular frequency ω_c as:

$$a=\frac{2.34\beta}{\omega_c} \tag{26}$$

The stress drop, average dislocation and other focal parameters can then be solved from Eqn. (27).

$$\begin{cases}\Delta\sigma=\dfrac{7m_0}{16a^3}\\ \Delta\bar{u}=\dfrac{16\Delta\sigma\cdot a}{7\pi\mu}\\ \Delta u_m=\dfrac{3\Delta\bar{u}}{2}\end{cases} \tag{27}$$

2.4.2 Explosive source model

The hypocentral radius and stress drop can also be solved in frequency domain using two ways. The first way is to use the displacement response spectrum of P-wave and removing the influences of instruments and medium to obtain the P-wave spectrum at the hypocenter.

$$\begin{cases}\left|\hat{u}_\alpha(0)\right|=\dfrac{a^3\cdot\Delta\sigma}{8\pi\mu r\alpha}\\ f_c=\dfrac{\alpha}{\sqrt{3}\cdot\pi a}\end{cases} \tag{28}$$

Next, plot the spectrum in a logarithmic chart and calculate the hypocentral radius a from the corner frequency f_c, the stress drop $\Delta\sigma$ can be eventually solved from a and the low-frequency level $\hat{u}_\alpha(0)$.

An alternative method is to directly plot a logarithmic chart for the recorded P-wave displacement spectrum and eliminate the instrumental influence to have:

$$\lg\frac{\left|\hat{R}_\alpha(\omega)\right|}{\left|\hat{I}(\omega)\right|}=\frac{\lg\left|\hat{u}_\alpha(\omega)\right|}{r}-\omega\cdot\frac{\lg e}{2Q\alpha}\cdot v_\varphi\cdot\left(t_S-t_P\right) \tag{29}$$

In above equation v_φ is virtual wave velocity, t_S and t_P are arrival times of S- and P-wave, respectively. In the diagram, the low-frequency part (< f_c) are fitted using a straight line and the medium quality factor Q then can be obtained from its slope. The low-frequency level $\hat{u}_\alpha(0)$ is estimated from the intercept of that fitting line. Based on those results, the hypocentral radius a and stress drop $\Delta\sigma$ finally can be solved.

3 Methods for Solving Rupture Characteristics

3.1 Unilateral Finite Moving Source Model

The far-field P-wave displacement spectrum of unilateral finite moving source can be described as:

$$\begin{cases}\hat{u}_\alpha(r,\omega)=\dfrac{m_0}{4\pi\rho\alpha^3 r}\Re_j\cdot F(\alpha)\cdot\Omega_\alpha(\omega)\\ \Omega_\alpha(\omega)=i\omega\cdot\hat{G}(\omega)\cdot e^{-i\frac{\omega r}{\alpha}-iX}\cdot\dfrac{\sin X}{X}\\ X=\dfrac{\omega L}{2}\left(\dfrac{1}{v_f}-\dfrac{\cos\psi}{\alpha}\right)\\ F(\alpha)=\dfrac{1}{1-\dfrac{v_f\cdot\cos\psi}{\alpha}}\end{cases} \tag{30}$$

Its low-frequency asymptote is the same as that of the shear dislocation circle. There are a series of local minimums. The period corresponding to the first local minimum T_1 is:

$$T_1=L\left(\frac{1}{v_f}-\frac{\cos\psi}{\alpha}\right) \tag{31}$$

Seismic moment m_0 can be obtained from the low-frequency level $\hat{u}_\alpha(0)$ of the source P-wave displacement spectrum.

$$m_0=4\pi\rho\alpha^3 r\cdot\left|\hat{u}_\alpha(0)\right|/\Re_\alpha \tag{32}$$

Length of rupture plane L and rupture speed v_f can be determined from the slope and intercept of T_1-cosψ lines recorded by multiple seismic observatories. Rupture propagation direction is the direction along which the period decreases.

Based on m_0 and L, the average dislocation $\Delta\bar{u}$, maximum dislocation $\Delta u_{\max}$, average strike-slip dislocation and stress drop $\Delta\bar{u}_{(s)},\Delta\sigma_{(s)}$, and average dip-slip dislocation and stress drop $\Delta\bar{u}_{(d)},\Delta\sigma_{(d)}$ can be obtained.

$$\begin{cases} \Delta u = \dfrac{m_0}{\mu \cdot S} \\ \Delta u_{\max} = \dfrac{4}{\pi}\Delta\bar{u} \\ \Delta\bar{u}_{(s)} = \Delta\bar{u} \cdot \cos\lambda \\ \Delta\bar{u}_{(d)} = \Delta\bar{u} \cdot \sin\lambda \\ \Delta\sigma_{(s)} = \dfrac{\mu \cdot \Delta u_{\max(s)}}{W} \\ \Delta\sigma_{(d)} = 2\mu\dfrac{\lambda+\mu}{\lambda+2\mu} \cdot \dfrac{\Delta u_{\max(d)}}{W} \end{cases} \tag{33}$$

where W is the width of the fault plane which can be assumed as double focal depth (W = 2h); S is the area of the fault plane (S = W × L); λ is the slip angle of the fault plane; subscripts (s) and (d) denote the strike-slip and dip-slip components, respectively.

3.2 Bilateral Finite Moving Source Model [3]

Focal P-wave displacement spectrum in frequency domain can be obtained from Eqn. (34)

$$\begin{cases} \hat{u}_\alpha(r,\omega) = \dfrac{m_0}{4\pi\rho\alpha^3 r}\Re_\alpha \cdot i\omega \cdot \hat{G}(\omega) \cdot e^{i\frac{\omega r}{\alpha}}\left(\dfrac{L_0}{L}e^{-iX_0} \cdot \dfrac{\sin X_0}{X_0} + \dfrac{L_\pi}{L}e^{-iX_\pi} \cdot \dfrac{\sin X_\pi}{X_\pi}\right) \\ L = L_0 + L_\pi \\ X_0 = \dfrac{\omega L_0}{2}\left(\dfrac{1}{v_f} - \dfrac{\cos\psi}{\alpha}\right) \\ X_\pi = \dfrac{\omega L_\pi}{2}\left(\dfrac{1}{v_f} + \dfrac{\cos\psi}{\alpha}\right) \end{cases} \tag{34}$$

Figure 3 plots local minimums of the P-wave spectrum, which is obtained from theoretical displacement spectrum of P-wave.

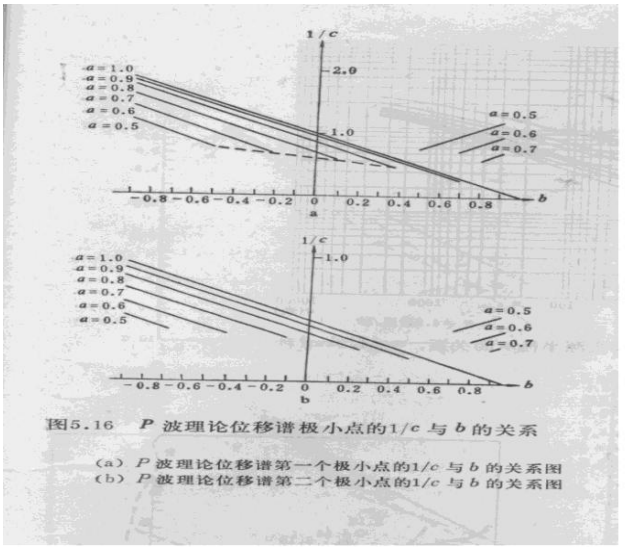

Figure 3: Relationships of 1/c of the first and second minimum to b

In above figure, a, b, c, and f are defined as

$$\begin{cases} a = \dfrac{L_0}{L} \\ b = \dfrac{v_f \cos\psi}{\alpha} \\ c = \dfrac{fL}{v_f} \\ f = \dfrac{\omega}{2\pi} \end{cases} \tag{35}$$

Figure 3 shows that:

(1) Periods of the first and second minimums are linearly related to cosψ

$$\begin{cases} T_{\min}^{1} = n_1 \dfrac{L}{v_f} - \dfrac{L}{\alpha}\cos\psi \\ T_{\min}^{2} = n_2 \dfrac{L}{v_f} - 0.5\dfrac{L}{\alpha}\cos\psi \end{cases} \tag{36}$$

(2) 1/c reduces to disappear with d increases and the point of disappear is the inflexion. Beyond the inflexion, 1/c reappears with the increasing d while the correlation between 1/c and b is changed.

The steps of solving for m_0, L_0, L_π, v_f, $\Delta\bar{u}$, $\Delta\sigma$ are

(1) Determine m_0 from low-frequency asymptote, $m_0 = 4\pi\rho\alpha^3 r \cdot \left|\hat{u}_\alpha(0)\right| / \Re_\alpha$.

(2) Determine L from the slope of T_{min}^{1}-cosψ curves in spectra obtained from multi observatories.

(3) Compare the spectra of multi observatories to find the inflexion and determine its ψ_c and f_c, and calculate Z using Eqn. (37)

$$Z = \left(\frac{1/f_c}{\cos\psi_c}\right)\left(\frac{a}{L}\right) \tag{37}$$

(4) Find a from Z according to Table 3.
(5) Find n_1, n_2 from a according to Table 4.
(6) Calculate L_0 and L_π from L and a using Eqn. (35).
(7) Determine v_f from the interception of T_{min}^{-1}-cosψ curves obtained from multi observatories.
(8) Calculate the average dislocation $\Delta\bar{u}$, maximum dislocation Δu_{max}, average strike-slip dislocation and stress drop $\Delta\bar{u}_{(s)}, \Delta\sigma_{(s)}$, and average dip-slip dislocation and stress drop $\Delta\bar{u}_{(d)}, \Delta\sigma_{(d)}$ from m_0 and L using Eqn. (33).

Table 3

a	0.5	0.6	0.7	0.8
b	-0.5	-0.2	0.1	0.4
1/c	0.76	0.69	0.59	0.46
Z	-1.52	-3.45	5.9	1.15

Table 4

a	1	0.9	0.8	0.7	0.6	0.5
n_1	1	0.97	0.87	0.699	0.508	0.24
n_2	0.5	0.46	0.4	0.31	0.2	0.07

3.3 Determine Rupture Characteristics Using Directional Function [4]

Earthquake's rupture characteristics include unilateral rupture or bilateral rupture, and the primary rupture direction for unilateral rupture. Considering an asymmetric bilateral rupture (Fig. 4), whose rupture propagation velocity is v_f, rupture lengths of two sides are L_0 and L_π, focal depth h = 0, and the seismic observatory's epicentral distance is r. The far-field radiation's P-wave spectrum on the seismic observatory is

$$\hat{u}_\alpha(\omega) = \frac{m_0}{4\pi\rho\alpha^3 r}\Re_\alpha i\omega\hat{G}(\omega)e\frac{i\omega r}{\alpha}\left(\frac{L_0}{L}e^{-ix_0}\cdot\frac{\sin x_0}{x_0} + \frac{L\pi}{L}e^{-ix_\pi}\cdot\frac{\sin x_\pi}{x_\pi}\right) \tag{38}$$

where

$$\begin{cases} X_0 = \dfrac{\omega L_0}{2}\left(\dfrac{1}{v_f} - \dfrac{\cos\theta}{\alpha}\right) \\ X_\pi = \dfrac{\omega L_\pi}{2}\left(\dfrac{1}{v_f} + \dfrac{\cos\theta}{\alpha}\right) \\ \Re_\alpha = \sin 2\theta \\ L = L_0 + L_\pi \end{cases} \tag{39}$$

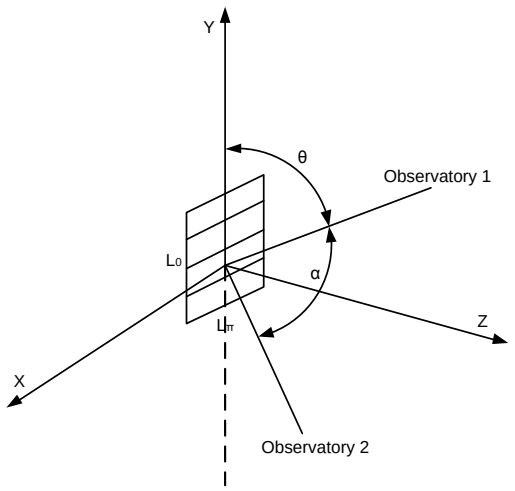

Figure 4: Asymmetric bilateral rupture

If an earthquake was recorded by seismic observatory 1 and 2, and the epicentral distances of the two observatories were equal to each other. Assuming the two stations located on two lines emanated from the hypocenter along reverse directions, the ratio between the amplitude spectrums obtained from the two observatories can be defined as the directional function D:

$$D = \frac{|\hat{u}_1(\omega)|}{|\hat{u}_2(\omega)|} = \frac{\left| e^{-ix_{10}} \sin x_{10}\left(\frac{1}{v_f} + \frac{\cos\theta}{\alpha}\right) + e^{-ix_{1\pi}} \sin x_{1\pi}\left(\frac{1}{v_f} - \frac{\cos\theta}{\alpha}\right)\right|}{e^{-ix_{20}} \sin x_{20}\left(\frac{1}{v_f} + \frac{\cos\theta}{\alpha}\right) + e^{-ix_{2\pi}} \sin x_{2\pi}\left(\frac{1}{v_f} - \frac{\cos\theta}{\alpha}\right)} \tag{40}$$

Obviously, D is a function of ω with parameters L_0/L and θ.

If the field angle between the lines from both observatories to the epicenter is denoted as ϕ (ϕ ≠ π), then the ratio between the two amplitude spectrums can be defined as the generalized directional function D_G

$$D_G = \frac{\left|\sin 2\theta\left(\frac{1}{v_f} + \frac{\cos(\theta+\varphi)}{\alpha}\right)\left(\frac{1}{v_f} - \frac{\cos(\theta+\varphi)}{\alpha}\right)\right|}{\left|\sin 2(\theta+\alpha)\left(\frac{1}{v_f} + \frac{\cos\theta}{\alpha}\right)\left(\frac{1}{v_f} - \frac{\cos\theta}{\alpha}\right)\right|} \cdot \frac{\left|e^{-ix_{10}}.\sin x_{10}\left(\frac{1}{v_f} + \frac{\cos\theta}{\alpha}\right) + e^{-ix_{1\pi}}.\sin X_{1\pi}\left(\frac{1}{v_f} - \frac{\cos\theta}{\alpha}\right)\right|}{\left|e^{-ix_{20}}.\sin x_{20}\left(\frac{1}{v_f} + \frac{\cos(\theta+\varphi)}{\alpha}\right) + e^{-ix_{2\pi}}.\sin X_{2\pi}\left(\frac{1}{v_f} - \frac{\cos(\theta+\varphi)}{\alpha}\right)\right|} \tag{41}$$

Similarly, D_G is a function of ω with parameters ϕ, L_0/L and θ.

In determining the primary rupture direction based on 2 observatories' records, we first measure the field angle α. Next, we choose 6 L_0/L values from 0.5 to 1.0 with increment 0.1 and 12 θ values from 0º to 180º with equal increment 15º. Based on these parameters, 6 × 12 = 72 generalized directional function curves can be obtained. The calculated curves are then compared with the curve recorded by the observatory 1 to find the closest calculated curve and corresponding L_0/L and θ values. Two candidate primary rupture directions can be obtained by adding/subtracting the θ to/from the observatory 1's geographic azimuth, one of which must be the true primary rupture direction. If more than 3 observatories' records are available, we will be able to obtain more than 2 generalized directional functions D_G and more than 4 candidate primary rupture directions following

the same method. These candidate directions and rupture azimuths are counted based on 4 quadrants, and the quadrant where most rupture azimuths are located is selected. The average value of these selected rupture azimuths is then calculated and specified as the earthquake's primary rupture direction. Fig. 5 plots the generalized directional function curves with different L_0/L and θ values, which were calculated for the Ms3.3 earthquake occurred at 4:44 on October 2nd in 1986 based on records from Nanjing and Bengbu observatories. Theoretical curves are also shown in that figure and compared to the calculated curves to determine that θ = 60º and L_0/L = 0.90.

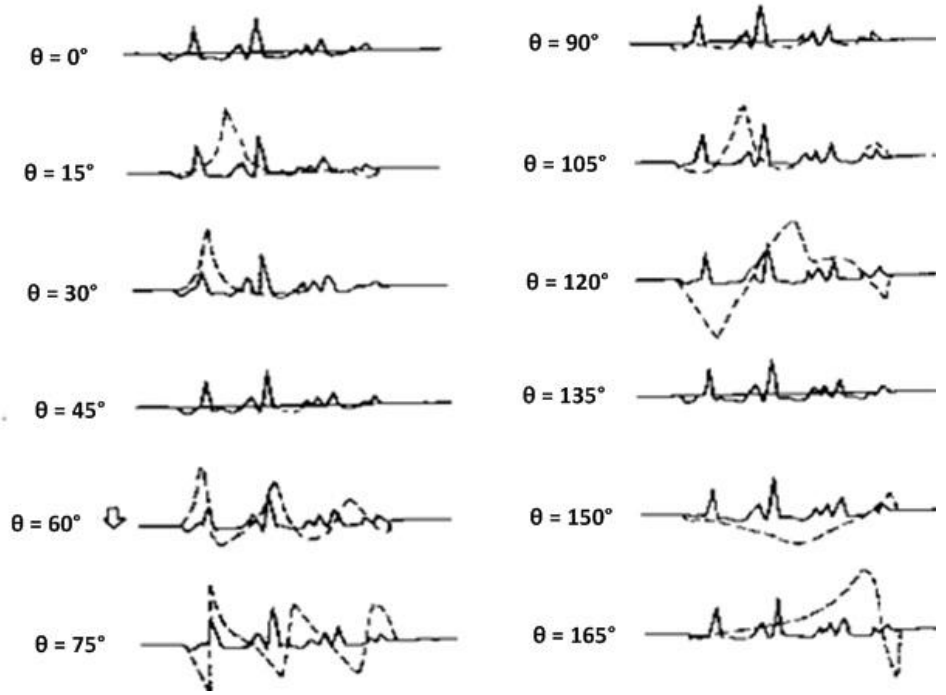

Figure 5: Comparison of calculated generalized directional function curves D_G and its theoretical curves

4 Methods for Solving Q Value of Medium

The quality factor of medium, Q, is a dimentionless parameter that describes the seismic wave absorption capability of the medium. It is defined as reciprocal of the ratio of the energy loss within a distance of one wavelength and the total energy. In laboratory, it is measured as:

$$Q^{-1} = \frac{\Delta\omega}{2\pi\omega} \tag{42}$$

In that equation Δω is the sample's energy loss during a stress cycle; ω is the stored elastic energy when the sample's strain reaches maximum. The seismic wave's amplitude attenuates with respect to distance r with attenuation coefficient α.

$$A = A_0 e^{-i\alpha r} \tag{43}$$

Q is related to α, frequency f, and wave velocity c as:

$$Q = \frac{\pi \cdot f}{\alpha \cdot c} \tag{44}$$

Several ways of solving Q from the seismic wave are presented here.

Method 1: Based on Eqn. (29), Q can be calculated as:

$$Q = \frac{\lg e \cdot v_{\varphi} \cdot \left(t_{\bar{S}} - t_{\bar{P}}\right)}{2K \cdot \alpha} \tag{45}$$

where K is the slope of high-frequency asymptote, e is the base of the natural logarithm, v_{φ} is the velocity of virtual wave, and $t_{\bar{S}}, t_{\bar{P}}$ are the arrival time of S and P wave, respectively.

Method 2: The frequency spectrum of body wave is $A(\omega) = A_0(\omega)\exp\left(-\frac{\omega t}{2Q}\right)$, for a recorded earthquake, we find frequency spectrum ratio of two frequencies ω_1 and ω_2 as:

$$\ln \frac{|A(\omega_1)|}{|A(\omega_2)|} = \ln \frac{|A_0(\omega_1)|}{|A_0(\omega_2)|} - \frac{\omega_1 - \omega_2}{2} \cdot \frac{t}{Q} \tag{46}$$

That ratio can be assumed as a constant if these earthquakes occurred in the same area with magnitudes were close to each other, the average Q in that area then can be determined from the slope K of the curve $\ln(|A(\omega_1)|/ |A(\omega_2)| \sim t$.

$$\overline{Q} = \frac{\omega_1 - \omega_2}{2K} \tag{47}$$

Method 3: If an earthquake is recorded by two observatories then Q value can be determined from travel times of the two observatories t_1, t_2 and the frequency spectrum ratio defined in Eqn. (46), which is:

$$\ln \frac{|A(\omega)_1|}{|A(\omega)_2|} = \frac{\omega(t_2 - t_1)}{2Q} \tag{48}$$

Method 4: Q can also be estimated from the attenuation of the seismic surface wave between two observatories as [5]:

$$Q(\omega_j) = \frac{\omega_j}{2v_j}(\Delta_2 - \Delta_1) / \ln\left(\frac{A_{1,j}\sqrt{\sin\Delta_1}}{A_{2,j}\sqrt{\sin\Delta_2}}\right) \tag{49}$$

where A is the calibrated amplitude; Δ is the epicentral distance (in degree); v is the group velocity of the seismic wave; subscripts 1 and 2 represent the observatories; subscript j means that it is related to the surface wave with angular frequency ω_j. It can be seen from Eqn. (49) that the calculated Q is related to the frequency of selected surface waves. Surface waves with different frequencies can penetrate the Earth's crust with different depths and some waves can even reach the upper mantle. Thus, the variation of Q with respect to frequency also reflects its variation with respect to the depth.

Method 5: Using attenuation characteristics of S and SS waves which are recorded by same observatory to evaluate the Q value as [6]:

$$Q = 0.4343\Delta T / 2K \tag{50}$$

In above equation, ΔT is the difference of arrival times of S and SS waves; K is slope of the line

$$\lg \frac{A(\omega)}{A'(\omega)} = C + K\omega \tag{51}$$

where A(ω) and A'(ω) are amplitude spectra of S and SS wave in that observatory.

Method 6: Evaluate Q using $f_p \sim t^*$ of seismic coda wave [7]. For small earthquake, by neglecting its source, the amplitude of its coda wave is:

$$A(f, t^*) = K \cdot I(f) \cdot e^{-\pi \cdot f \cdot t^*} \text{ and } t^* = r / Q \tag{52}$$

The maximum amplitude can be found from above equation by setting $\partial A/\partial f = 0$, where the frequency f is the predominant frequency f_p, from which the $f_p \sim t^*$ relationship can be obtained as:

$$t^* = \frac{d \ln I(f_p)}{\pi \cdot df_p} \tag{53}$$

From above equation, the theoretical $f_p \sim t^*$ plot of the used instruments can be drawn. From the diagram of a coda wave to evaluate an f_p by counting the number of time that the waveform passes through zero line within a specified time period (such as 10 seconds) from the origin time and dividing that number by double time period, an observation $f_p \sim t$ curve then can be plotted. That observation curve is then matched with the theoretical curve obtained from Eqn. (53), the Q value becomes the value of t on the observation curve at $t^* = 1$.

Method 7: Alternatively, the $f_p \sim t^*$ relationship can be determined from the coda wave's shape function $C(f_p, t^*)$ of the used instrument, which is calculated as:

$$C(f_p, t^*) = I(f_p) \cdot t^{*-\frac{1}{2}} \cdot \left(\frac{df_p}{dt^*} \right)^{\frac{1}{4}} \cdot \exp(-\pi f_p \cdot t^*) \tag{54}$$

The Q value then can be determined following the approach presented in method 6.

Method 8: The Q value can also be evaluated using attenuation coefficient of the coda wave, α. The shape of envelope curve of attenuation of the coda wave A(t) is defined in Eqn. (55), and from α, the quality factor Q of the coda wave can be calculated using Eqn. (56).

$$\lg A(t) = C - 0.5 \lg t - \alpha t \tag{55}$$

where:

$$\left.\begin{aligned} C &= \frac{1}{2} \lg \left[\frac{\Delta\omega}{\pi} \cdot 1.23 (n_0 \sigma_r)^2 \cdot S(\omega_0) \right] + 0.33 n_0 \sigma_r \lg e \\ \alpha &= \omega_0 \lg e / 2Q_C \end{aligned}\right\} \tag{56}$$

5 Error Analysis

Error analysis is an indispensable step in a complete study, without which obtained solutions cannot be used for any further analyses. In seismic analysis, the error is caused by various reasons and affected by different factors.

5.1 Error caused by Digitization

Digitization is the representation of the original analog curve f(t) with a discrete set of its points sampled at equal time intervals. The maximum error caused by the discretization Δf is:

$$\Delta f = \frac{(\Delta t)^2}{8} \mid f''(x) \mid_{max} + \frac{A}{2} \tag{57}$$

where A is the digitization precision. Resolution ratio of a scanner is 300 dpi and the dot pitch is 0.085 mm. Compared to the thickness of the recorded curve, it is the secondary factor that affects the precision of digitization. Given a thickness is 0.1mm and A is assumed to be half of the thickness, which is 0.05 mm. The acceleration at a distance of 200 km from epicenter of the earthquakes with magnitude about Ms3 will not exceed 10 mm/s^2. Assuming $|f''(t)|_{max} = 2.5$, the sampling rate is 300 dots during 12.7 seconds, and $\Delta t = 0.085$ mm, Δf can be calculated as 0.052 mm from above equation. Meanwhile, errors caused by large amplitude have to be calibrated in pretreatment process.

5.2 Error caused by the Simplified Source and Medium Model

In general source models, it is always assumed that the focal depth is 0. Therefore the radiation pattern factor R_α is simplified as $R_\alpha = \sin2\theta\cos\phi = \sin2\theta$. If the actual focal depth is 15 km and the epicentral depth is 200 km, we have $R_\alpha = \sin2\theta\cos[\arctan(15/200)] = 0.9972\sin2\theta$. The relative error is only 0.28%. Also, other factors such as the uneven distribution of the medium's Q value, assumption of the reflection coefficient of the earth's surface as 2, and incomplete instrumental calibration may also cause the error.

5.3 Errors Generated in Making Theoretical Template

For example, in plotting generalized directional function curves, we used to plot a theoretical curve for θ values from 0º to 180º every 15º. This means that the maximum error generated in that process could be 15°.

5.4 Errors Influenced by Distribution of the Local Observatories

If the used data was recorded by a number of observatories, the more evenly the observatories distribute and the larger the larger the field angles are, the smaller the error will be. Here we discuss the influence of the distribution of local observatories on the error of measured ambient shear stress τ_0 [8].

In evaluating the ambient stress, it is assumed that the average stress field reduced to zero in a large range after the earthquakes (which means that the friction between the fault planes can be neglected) and the yield strength of crust is 200 MPa, which value was measured in lab. The reliability of above assumptions still needs to be verified and in this paper we only discuss the relative accuracy of τ_0 obtained for different earthquakes.

According to [8] and take constant values $\upsilon = 0.252$, $\eta = 0.05$, $\mu = 33$GPa, we have:

$$\tau_0 = 10^{0.75M_s - 1.5\lg(2a) - 0.77} \tag{58}$$

Since the allowable error in measuring M_s is 0.3, therefore the error of τ_0 is:

$$(\tau + \Delta\tau) = 10^{0.75(m_s+0.3) - 1.5\lg(2a) - 0.77} = 10^{0.75\times0.3}\tau = 1.7\tau \tag{59}$$

which shows that the relative error $\Delta\tau_0/\tau_0$ can reach 70%.

If the error of focal radius a is k, from Eqn. (58) the induced error in τ_0 will be $k^{1.5}$. The error in a is composed of two errors. The first error is caused by the using of mean value of sinθ on the focal sphere for evaluating the radiation pattern factor:

$$t_{2\alpha} = a\left(\frac{1}{v_f} + \frac{\sin\theta}{v_p}\right) \tag{60}$$

By using the mean value of sinθ on the focal sphere, above equation becomes:

$$t_{2\bar{\alpha}} = a\left(\frac{1}{v_f} + \frac{\pi}{4v_p}\right) \tag{61}$$

Let $v_f = 0.775\beta$ and assume that $\beta = 3.38$ km/s, one can have:

$$\frac{|\bar{a} - a_{\max}|}{a_{\max}} = \frac{\left| t_{2\alpha} \Big/ \left(\frac{1}{v_f} + \frac{\pi}{4v_p}\right) - t_{2\alpha} \Big/ \left(\frac{1}{v_f} + \frac{1}{v_p}\right)\right|}{t_{2\alpha} \Big/ \left(\frac{1}{v_f} + \frac{1}{v_p}\right)} \approx 0.073 \tag{62}$$

$$\frac{|\bar{r}_h - (r_h)_{min}|}{(r_h)_{min}} = \frac{\left| t_{2\alpha} \Big/ \left(\frac{1}{v_f} + \frac{\pi}{4v_p}\right) - t_{2\alpha} \Big/ \left(\frac{1}{v_f}\right)\right|}{t_{2\alpha} \Big/ \left(\frac{1}{v_f}\right)} \approx 0.265 \tag{63}$$

In above equation, v_p is taken as 5.7 km/s in order to estimate the extreme error. Also we use $\bar{a}$ to denote the focal radius evaluated using the average sinθ on the focal sphere, a_{max} to denote the radius evaluated using the maximum sinθ = 1, and a_{min} to denote the radius evaluated using the minimum sinθ = 0. It can be calculated that when sinθ = 1, the error of τ_0 is $0.073^{1.5} \approx 2.0\%$, while sinθ = 0, the error becomes $0.265^{1.5} \approx 13.7\%$. Thus, the relative error caused by neglecting θ ranges from 2.0% to 13.7%.

Another error is measurement error. As demonstrated in previous sections, a can be determined based on the corner frequency $f_{c\alpha}$. In measuring $f_{c\alpha}$, if sampling step Δt is 0.0425 seconds, the folding frequency (23.5 Hz) is well above $f_{c\alpha}$, therefore the influence of high frequency aliasing can be neglected. Next, we chose the window length T = 4s and then the resolution is 1/4Hz. For an earthquake whose magnitude is about M3.0 and whose epicentral distance is 200km, the corner frequency $f_{c\alpha}$ will be around 2.5Hz. Thus, the relative error of $f_{c\alpha}$ may reach 0.1. Substituting this value into Eqn. (61) and (64), it can be found that the resulted relative error in a is $1/(1 + 0.1) \times 100\% \approx 9.1\%$. The consequent relative error in τ_0 is $0.091^{1.5} = 2.7\%$. Based on above discussion, it can be concluded that the errors in evaluating ambient stress τ_0 are mainly caused by the error in earthquake magnitude M_s and that error can reach 70%.

$$f_{c\alpha} = 0.60 / t_{\bar{2\alpha}} \tag{64}$$

6 Conclusions

A number of physical models and approaches are presented to solve for seismic source dynamic parameters as well as the medium's Q value. Errors in calculating those parameters are also discussed and methods for error analysis are illustrated as well. The paper shows that hypocentral radius, stress drop, and ambient shear stress can be solved using circular dislocation model, Brune model, explosive source model, or through instrumental and medium calibration. This paper also explains techniques used for earthquake selection, sampling and Fourier analysis. As for determining earthquake's rupture characteristics, the paper illustrates three methods: unilateral finite moving source model, bilateral finite moving source model, and directional function. Besides that, this paper also presents seven methods for computing Q value of medium. The methods and models demonstrated in this paper can be extensively used for investigating seismic wave parameters and therefore have wide prospect in earthquake prediction.

References

[1] J.D. Byerlee, "Static and Kinetic Friction of Granite at High Normal Stress", *International Journal of Rock Mechanics and Mining Science & Geomechanics Abstracts*, **7**(6), 1970, 577-582.

[2] Z.-K. Liu, W. Wang, R. Zhang, N.-H. Yu, T.-Z. Zhang, J.-Y. Pan, "A Seismogram Digitization and Database Management System", *ACTA Seismologica Sinica*, **23**(3), 2001.

[3] J.N. Brune, "Tectonic Stress and the Spectra of Seismic Shear Waves from Earthquakes", *Journal of Geophysical Research*, **75**(26), 1970, 4997-5009.

[4] B.-H. Liu, S.-F. Wu, Z.-M. Gao, "On the Lowering of the Epicentral Intensity of the Ninghe Aftershock of May 12, 1977", *Chinese Journal of Geophysics*, **22**(1), 1979, 14-24.

[5] W.-L. Liu, P.-Z. Wu, Y.-W. Chen, "Determination of Seismic Rupture Characteristics Using Directional Functions", *Earthquake Research in China*, **12**(1), 1996, 93-99.

[6] R. Feng, Z.-Q. He, "Q Value of Surface Waves in Eastern Region of Xizang Plateau", *Chinese Journal of Geophysics*, **23**(3), 1980, 291-297.

[7] L.-M. Zhang, Z.-X. Yao, "The Q-Value of the Medium of the Tibetan Plateau around Lasa Region", *Chinese Journal of Geophysics*, **22**(3), 1979, 299-303.

[8] R.B. Herrmann, "Q Estimates Using the Coda of Local Earthquakes", *Bulletin of Seismological Society of America*, **70**(2), 1980, 447-468.